Journal of Alloys and Compounds, 211/212 (1994) 66–70
JALCOM 041

Mechanical loss measurements on yttria- and calcia-stabilized zirconia

M. Weller
Max-Planck-Institut für Metallforschung, Institut für Werkstoffwissenschaft, D-70174 Stuttgart (Germany)

Abstract

In cubic ZrO_2 defects (oxygen vacancies) are created as a consequence of doping with lower valency cations (10 mol.% Y_2O_3 or 16 mol.% CaO) which are required for stabilization of the cubic phase. Mechanical loss measurements were applied on single crystals of cubic zirconia to study the local crystallographic structure of atomic defects. Specimens with different longitudinal axes ([100], [110], [111]) were measured in torsional ($f \approx 1$ Hz) and flexural oscillations ($f \approx 1$ kHz). A composite loss maximum consisting of two submaxima is observed: I (≈ 410 K) and I_A (≈ 510 K) in ZrO_2–Y_2O_3; I'(≈ 430 K) and I_A' (≈ 515 K) in ZrO_2–CaO ($f \approx 1$ Hz). The peak heights of maxima I and I' depend on specimen orientation as expected for a defect of trigonal ([111]) symmetry. This strongly points to oxygen vacancies located at nearest neighbour sites close to the dopant atoms which form elastic (and electric) dipoles, *i.e.* $(V_O^{\cdot\cdot}Y'_{Zr})^{\cdot}$ or $(V_O^{\cdot\cdot}Ca'')$-pairs, which are aligned parallel to ⟨111⟩ directions. The anelastic shape factor of the dipoles characterizing the anisotropy and strength of the local atomic displacements was determined as $\delta\lambda \approx 0.1$ for yttria-stabilized and $\delta\lambda \approx 0.05$ for calcia-stabilized zirconia. Loss maxima I_A and I_A' are assigned to larger clusters of oxygen vacancies with two or more dopant atoms.

1. Introduction

Pure zirconia (ZrO_2) exists in three well-defined polymorphs all of which are closely related to the cubic fluorite (CaF_2) structure. The monoclinic phase has a distorted fluorite structure and transforms into tetragonal ZrO_2 at about 1400 K. The tetragonality of this second phase is small (c/a ratio = 1.02) corresponding to a slightly stretched cubic structure. In pure ZrO_2 the cubic phase exists only above 2600 K. However, the cubic phase may be stabilized at ambient temperature by mixing ZrO_2 with lower valent rare earth or alkali oxides, *e.g.* $\gtrsim 8$ mol.% Y_2O_3 or $\gtrsim 16$ mol.% CaO. Such mixed (or doped) oxides exhibit superior ionic conductivity at elevated temperatures. This was detected in the previous century by Nernst [1] who used a mixture of zirconia and yttria as an electrical light source. Later on it was realized that zirconia is a solid electrolyte because of the presence of *oxygen vacancies*, and electrical charge transport occurs by hopping of oxygen ions via vacancies [2, 3]. For some time it has been possible to prepare tetragonal ZrO_2 with about 2–3 mol.% Y_2O_3 as a metastable phase at room temperature (RT) in the form of fine grained polycrystals (TZP).

The oxygen vacancies in cubic zirconia are created for electrical charge compensation because of doping with lower valent cations. In the commonly applied Kröger–Vink notation (see *e.g.* refs. 4 and 5) this may be represented by the following defect reactions:

$$Y_2O_3 \xrightarrow{ZrO_2} 2Y'_{Zr} + V_O^{\cdot\cdot} + 3O_O^{\times} \quad (1)$$

$$CaO \xrightarrow{ZrO_2} Ca''_{Zr} + V_O^{\cdot\cdot} + O_O^{\times} \quad (2)$$

Equations (1) and (2) indicate that one oxygen vacancy ($V_O^{\cdot\cdot}$ is created for every two Y^{3+} ions or for every Ca^{2+} ion (replacing Zr^{4+}).

The arrangement of cations and anions in the cubic fluorite structure is shown in Fig. 1. Figure 1(a) shows the face-centred cubic packing of the cations with the oxygen ions inside. The simple cubic packing of the

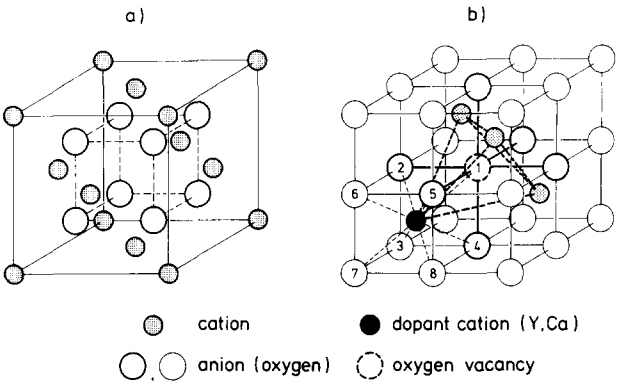

Fig. 1. Fluorite structure in different representations to demonstrate the coordination around the cations (a) and anions (b). The defect symmetry of an oxygen vacancy and its eight nearest neighbour sites around a dopant cation are indicated in (b).

SSDI 0925-8388(94)00041-V

oxygen ions is more clearly visible in Fig. 1(b). Note that only every second simple cube contains a cation in its centre. In Fig. 1(b) an oxygen vacancy is placed in the centre of the unit cell. In the fluorite lattice the oxygen vacancy represents an atomic defect with *cubic symmetry*. This may be derived from an inspection of the site symmetry of the defect including group theoretical considerations [6, 7]. The cubic symmetry of the vacancy may also be seen from its environment in Fig. 1(b). The vacancy is surrounded by six oxygen ions which spread an octahedron with cubic symmetry. The next four cations are located on a tetrahedron, also with cubic symmetry. Since the oxygen vacancy represents a cubic (isotropic) defect in the cubic host lattice we do not expect occurrence of mechanical (or dielectric) relaxation [6, 7] by hopping of isolated vacancies.

Mass transport, *i.e.* self-diffusion or ionic conduction, in ZrO_2 and other oxides with the fluorite structure (CeO_2, ThO_2, HfO_2) occurs via vacancies. The migration energies of vacancies in the fluorite lattice are rather low (0.5–1 eV) thus enabling fast oxygen diffusion at elevated temperatures. This is the basis for numerous technical applications (mostly with stabilized ZrO_2), as, for example, in fuel cells or gas sensors. At lower temperatures the +2 charged $V_O^{\cdot\cdot}$ become trapped by the oppositely charged dopant ions and the following defect associates (complexes) are formed

$$Y_{Zr}' + V_O^{\cdot\cdot} \rightleftharpoons (Y_{Zr}'V_O^{\cdot\cdot})^{\cdot} \quad (1a)$$

$$Ca''_{Zr} + V_O^{\cdot\cdot} \rightleftharpoons (Ca''_{Zr}V_O^{\cdot\cdot})^{x} \quad (2a)$$

Contributing to mass transport of the vacancies at lower temperatures requires that they be detached from the dopant ions thus leading to a higher activation enthalpy for diffusion or ionic conductivity than at higher temperatures. This behaviour becomes apparent in the temperature variation of ionic conductivity of doped oxides (and other ionic crystals). The conductivity at high temperatures (dissociated vacancies) is determined by a lower activation enthalpy than at low temperatures (associated vacancies) [8–10].

Oxygen vacancies, which are associated with dopant atoms, constitute defect pairs which have lower symmetry than the cubic host lattice. The oxygen vacancy in Fig. 1(b) is sited in a nearest neighbour position to the dopant ion and constitutes an elastic (and electric) dipole. Reorientation of the dipole may occur by jumping of the vacancy around the dopant ion. As a consequence, such "associated vacancies" may cause anelastic and dielectric relaxation – contrary to isolated vacancies. In fact, Wachtman [11] and Nowick and coworkers [8, 12] observed mechanical and dielectric loss maxima in CaO-doped ThO_2 and in Y_2O_3-doped CeO_2 which they assigned to defect associates (complexes) of oxygen vacancies with dopant atoms. They also concluded from their experiments that the oxygen vacancy is positioned on one of the eight nearest neighbour sites around the dopant atom (see Fig. 1(b)). This was derived from the observation that the relaxation times for anelastic and dielectric relaxation differ by a factor of two as expected from theory for this defect configuration [6, 8].

Another prediction of this "8-position model", the trigonal (⟨111⟩) defect symmetry, which results from the ⟨111⟩-orientation of the dipole axis could not be verified up to now since suitable monocrystals, which are necessary for such studies, were not available. This prompted us to carry out the present studies on cubic stabilized zirconia.

2. Experimental results

The crystals of yttria- and calcia-stabilized zirconia were supplied by the Ceres Corporation (North Billerica, MA, USA). The larger ZrO_2–10 mol.% Y_2O_3 crystal allowed preparation of longer specimens with dimensions of about $40 \times 5 \times 1$ mm^3 and with three different orientations of the longitudinal axis [100], [110] or [111]. The specimens from ZrO_2–16 mol.% CaO with [110] and [111] orientations and dimensions of about $25 \times 5 \times 1$ mm^3 were prepared from two crystals with smaller size.

Low frequency ($f \approx 3$ Hz) internal friction measurements were performed with an inverted torsion pendulum by exciting the specimens to torsional (shear) oscillations around their longitudinal axis. High frequency measurements ($f \approx 3$ kHz) were carried out by applying the resonant bar technique with flexure oscillations. For details see ref. 13.

Measurements of yttria-stabilized zirconia are shown in Figs. 2 and 3. Both the low frequency (Fig. 2) and high frequency measurements (Fig. 3) show a prominent loss maximum between 400 and 600 K. Obviously, the maximum is composed of two overlapping maxima which

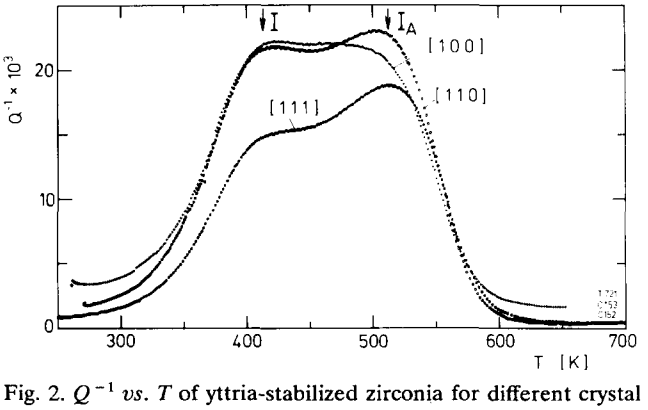

Fig. 2. Q^{-1} *vs.* T of yttria-stabilized zirconia for different crystal orientations (torsional oscillations with $f \approx 3$ Hz).

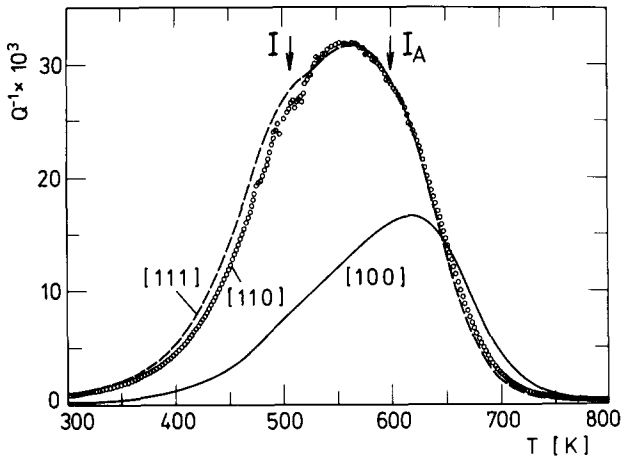

Fig. 3. Q^{-1} *vs.* T of yttria-stabilized zirconia (flexure oscillations with $f \approx 3$ kHz).

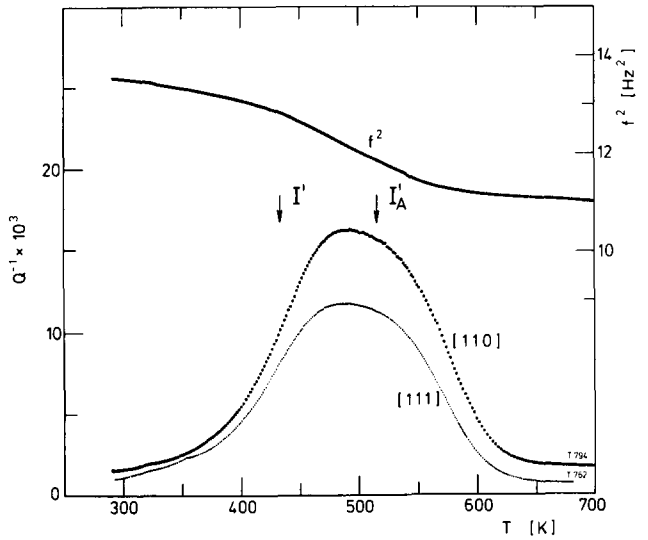

Fig. 4. Q^{-1} *vs.* T of calcia-stabilized zirconia (torsional oscillations, $f \approx 3$ Hz).

are designated with I and I_A. The height of the maxima varies with the orientation of the longitudinal axis.

Low frequency measurements ($f \approx 3$ Hz) for calcia-stabilized zirconia were shown in Fig. 4. A broad loss maximum appears which is also composed of two submaxima and which are designated with I' and I_A'. The resonant bar technique using kilohertz oscillations could not be applied for these relatively shorter specimens (25 mm length). The loss maximum in calcia-doped zirconia was observed earlier by Wachtmann and Corwin [14] and Pélaud *et al.* [15].

3. Analysis of loss spectra

3.1. Decomposition of the loss spectra

The loss spectra were decomposed into two Debye maxima according to:

$$Q^{-1}(T) \simeq \frac{\Delta}{2} \operatorname{sech}\left[\frac{\bar{H}}{k}\left(\frac{1}{T} - \frac{1}{T_p}\right)\right] \tag{3}$$

($\bar{H}$ = mean activation enthalpy, T_p = peak temperature) by neglecting the temperature dependence of the relaxation strength, $\Delta\,(T)$, and of the measuring frequency (modulus) $f(T)$ [16]. Since the loss maxima are about 2 to 3 times braoder than simple Debye maxima, a Gaussian distribution of relaxation times was introduced for every submaximum. The parameter β characterizing the width of the gaussian distribution is defined as in ref. 7. A non-linear regression procedure which is described in detail in ref. 16 was applied for decomposition of the loss spectra.

3.1.1. ZrO_2–Y_2O_3

The low frequency loss spectra in Fig. 2 gave the following results for the three crystal orientations: Maximum I: $T_p = 407$–420 K; $\beta \approx 4$. Maximum I_A: $T_p = 505$–518 K; $\beta \approx 3$. Decomposition of the loss spectra of the kilohertz flexural vibrations (Fig. 3) gave in a similar way:
Maximum I: $T_p = 504$–510 K; $\beta \approx 3$. Maximum I_A: $T_p = 590$–613 K; $\beta \approx 2$. All calculations were performed with $\bar{H} = 1$ eV for maximum I, and $\bar{H} = 1.3$ eV for maximum I_A (corresponding to $\tau_\infty = 10^{-14}$ s).

3.1.2. ZrO_2–CaO

The two loss maxima in calcia-stabilized zirconia (Fig. 4) are closer together. The fitting procedure gave the following results (two crystal orientations):
Maximum I': $T_p = 432$ and 434 K; $\beta = 2.6$ and 2.8.
Maximum I_A': $T_p = 511$ and 519 K; $\beta = 5.3$ and 4.3.

3.2. Calculation of relaxation amplitudes

The magnitude of relaxation, which determines the height of a loss maximum, is usually expressed as the relaxation amplitude. By using compliances, *i.e.* reciprocals of moduli, the relaxation amplitudes for shear oscillations, δG^{-1}, and flexure oscillations, δE^{-1}, may be expressed as:

$$\delta G^{-1} = \Delta \cdot G^{-1};\ \delta E^{-1} = \Delta \cdot E^{-1} \tag{4}$$

(G = shear modulus, E = Young's modulus). The relaxation amplitudes are proportional to the concentrations of defects (c_o) and their dipole strength $\delta\lambda$ (anelastic shape factor). For simple defects in cubic crystals the following equations hold [6, 7]:

$$\delta G^{-1} = K_1 \cdot \frac{c_o v_o (\delta\lambda)^2}{kT} F_G(I) \tag{5a}$$

$$\delta E^{-1} = K_2 \cdot \frac{c_o v_o (\delta\lambda)^2}{kT} F_E(I) \tag{5b}$$

Here v_o is the molecular volume and K_1 and K_2 are numerical parameters near unity. Γ is the orientation parameter of the longitudinal specimen axis, $\Gamma = \cos^2\alpha\cos^2\beta + \cos^2\beta\cos^2\gamma + \cos^2\gamma\cos^2\alpha$ (α, β, γ = angles between longitudinal specimen axis and cubic directions). For example, $\Gamma = 0$ for a [100] orientation, and $\Gamma = 1/3$ for a [111] direction.

For simple atomic defects in cubic crystals F_G (Γ) and F_E (Γ) represent *linear* functions of the orientation parameter Γ. These functions contain information which is pertinent to the defect symmetry. For trigonal ([111]-oriented) defects in cubic crystals, we expect

$$F_G = 1 - 2\Gamma; \qquad F_E = \Gamma \tag{6}$$

and for defects with tetragonal symmetry

$$F_G = \Gamma; \qquad F_E = 3\,\Gamma - 1 \tag{7}$$

Decomposition of the loss spectra by applying the non-linear regression procedure [16] also gives values for the relaxation strength Δ of submaxima I and I_A, and I' and I_A', respectively, for different crystal orientations, *i.e.* different values of Γ. The relaxation amplitudes for various orientations may then be calculated with eqns. (4) and with appropriate values of the elastic moduli (see ref. 13). Figure 5 shows the relaxation amplitudes δG^{-1} and ΔE^{-1} for submaxima I and I_A' in yttria-stabilized zirconia. The results for

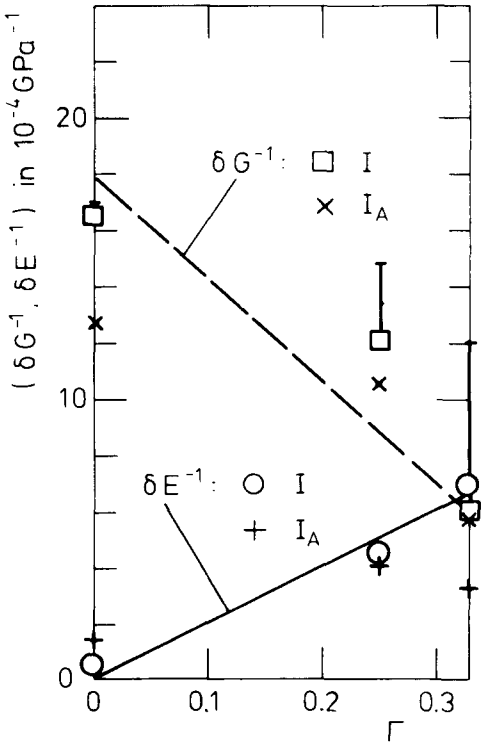

Fig. 5. Variation of relaxation amplitudes, δE^{-1} and δG^{-1}, of submaxima I and I_A with orientation parameter Γ for yttria-stabilized zirconia.

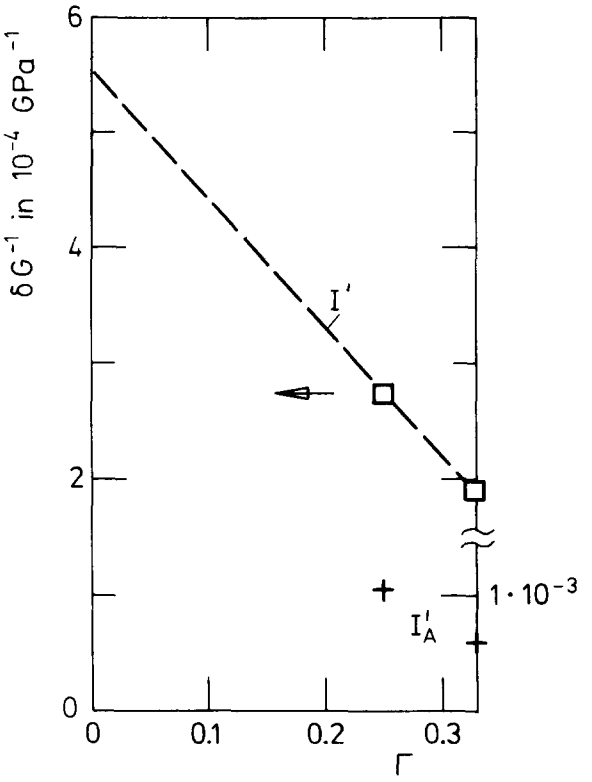

Fig. 6. Variation of relaxation amplitude, δG^{-1}, of submaxima I' and I_A' with Γ for calcia-stabilized zirconia.

δG^{-1} (only) in calcia-stabilized zirconia are shown in Fig. 6.

4. Discussion

The orientation dependence of the relaxation amplitudes of the loss maxima in cubic zirconia leads to the following conclusions:

(1) The relaxation amplitudes $\delta G^{-1}(\Gamma)$ and $\delta E^{-1}(\Gamma)$ of *maximum* I in ZrO_2–Y_2O_3 (Fig. 5) may well be approximated by linear equations $F(\Gamma)$ as expected for simple atomic defects. The orientation dependence of both relaxation amplitudes agrees well with that of *trigonal* ([111]-oriented) defects. The solid and dashed lines in Fig. 5 correspond to eqn. (6). For a tetragonal defect we would expect just the opposite behaviour (eqn. (7)). In ZrO_2–CaO the orientation dependence of *maximum* I' for the two orientations is also in agreement with a trigonal defect symmetry (dashed line in Fig. 6). *Maximum* I_A in ZrO_2–Y_2O_3 does not exhibit a linear relation between either δG^{-1} or δE^{-1} and Γ as expected for the simple atomic defects according to eqns. (6) or (7). This indicates that defects of lower symmetry and/or interaction of defects (agglomerates) may contribute to this relaxation.

(2) Apparently, loss maxima I and I' are due to elastic dipoles with trigonal symmetry. The shape factor $\delta\lambda$

describing the anisotropy of the distortion pattern may be determined from $\delta G^{-1}(I)$ or $\delta E^{-1}(I)$ (eqns. (5(a), 5(b)). For trigonal defects we have $K_1 = K_2 = 4/9$ [5–7]. We may assume further that the concentration of dipoles, c_0, corresponds approximately to that of oxygen vacancies $[V_O^{\cdot\cdot}]$. This may be estimated with the help of eqns. (1) and (2) from the dopant contents and by referring to the anion sublattice (*i.e.* $c_o \approx 0.075$ for yttria- and $c_o \approx 0.08$ for calcia-doped zirconia). With eqns. (5a) and (5b) we arrive at $\delta\lambda \approx 0.1$ for Y_2O_3- and $\delta\lambda \approx 0.05$ for CaO-doped ZrO_2.

(3) The trigonal symmetry of the defects causing maxima I and I' leads directly to their assignment to $(Y_{Zr}'V_O^{\cdot\cdot})^{\cdot}$ and $(Ca''V_O^{\cdot\cdot})^{x}$ associates in which the oxygen vacancies are positioned on the eight [111]-oriented neighbour positions around the dopant atom (see Fig. 1(b)).

The orientation dependence of loss maxima I and I' gives an excellent verification of the "8 position model" (see Fig. 1(b)). The assignment of maximum I in yttria-doped zirconia to $(Y_{Zr}'V_O^{\cdot\cdot})^{\cdot}$-dipoles is also in agreement with earlier results from TZP [17, 18]. For lower yttria contents (2–3 mol.%) an isolated loss maximum is observed at slightly lower temperatures ($T_p \approx 380$ K for 1 Hz, $\bar{H} \approx = 0.95$ eV) which correlates with a dielectric loss maximum with about equal activation enthalpy. The relaxation times differ by a factor of about two. The tetragonality of TZP is only about 1.02 thus allowing a direct comparison of results from cubic and tetragonal ZrO_2. In tetragonal zirconia the peak temperature, and thus the activation enthalpy for reorientation of dipoles, increases with yttria contents. This may explain the slightly higher peak temperature ($\simeq 410$ K) of maximum I in cubic zirconia with 10 mol.% Y_2O_3.

The existence of additional loss maxima (I_A, I_A') at higher temperatures may be quite naturally assigned to relaxation of oxygen vacancies within Y- or Ca-clusters, from which different types and configurations may exist. Interactions of the dipoles (defects) with each other as well as the existence of ordered or partly ordered domains may contribute to the broadening of the loss maxima.

5. Conclusions

Yttria- and calcia-stabilized zirconia exhibit a highly defective structure due to the high dopant concentrations required for stabilization. The orientation dependence of loss maxima I (ZrO_2–Y_2O_3) and I' (ZrO_2–CaO) indicates that the oxygen vacancies are predominantly associated in nearest neighbour positions with the dopant ions thus representing defects with trigonal symmetry (elastic dipoles). Agglomeration and defect interaction leads to additional loss maxima (I_A, I_A') which are positioned at higher temperatures than the dipole maxima I and I'.

References

1 W. Nernst, *Z. Elektrochem., 6* (1899) 41.
2 C. Wagner, *Naturwissenschaft 23/24* (1943) 265.
3 F. Hund, *Z. Elektrochem., 563* (1951) 363.
4 T. Kudo and K. Fueki, *Solid State Ionics*, Kodansha Ltd, Tokyo and VCH Verlagsgesellschaft, Weinheim, 1990.
5 M. Weller, *Mechanical and Dielectric Loss Spectroscopy of Defects in Oxides, International Summer School on Mechanical Spectroscopy, September 8–14, 1991, Cracow, Poland*, in L.B. Magalas (ed.), *Mechanical Spectroscopy,* in press.
6 A.S. Nowick and W.R. Heller, *Adv. Phys., 14* (1965) 101, and *16* (1967) 1.
7 A.S. Nowick and B.S. Berry, *Anelastic Relaxation in Crystalline Solids*, Academic Press, New York, 1972.
8 A.S. Nowick, in G.E. Murch and A.S. Nowick (eds.), *Diffusion in Crystalline Solids*, Academic Press, New York, 1984, p. 43.
9 A.B. Lidiard, in S. Flügge (ed.), *Handbuch der Physik*, Vol. 20, II, Springer Verlag, Berlin, 1957, p. 246.
10 J.A. Kilner and C.D. Waters, *Solid State Ionics, 6* (1982) 253.
11 J.B. Wachtman, *Phys. Rev., 131* (1963) 517.
12 M.P. Anderson and A.S. Nowick, *J. de Phys., 42* (1981) 823.
13 M. Weller, *Z. Metallkd., 84* (1993) 381.
14 J.B. Wachtman and W.C. Corwin, *J. Res. NBS, A, Phys. & Chem., 69A* (1965) 457.
15 S. Pélaud, P. Mazot and J. Woirgard, *J. Phys. (France), 51* (1990) 1979.
16 G. Haneczok and M. Weller, *J. Less. Common Met., 159* (1990) 269.
17 M. Weller and H. Schubert, *J. Am. Ceram. Soc., 69* (1986) 573.
18 M. Weller and H. Schubert, in M. Balkanski, T. Takahashi and H.L. Tuller (eds.), *Solid State Ionics,* Elsevier, Amsterdam, 1990, p. 569.